NUMERICAL SOLUTION OF A FÖPPL–VON KÁRMÁN MODEL

SÖREN BARTELS

ABSTRACT. The formation of folds and ridges in the elastic deformation of thin elastic sheets is related to certain instabilities in mathematical models derived from continuum mechanics. Their approximation is difficult due to nonuniqueness and localization effects which result from nonlinearities and singular perturbations. Numerical methods for simulating these effects have to be justified without unrealistic assumptions on exact solutions. The paper proposes a convergent finite element discretization of a Föppl–von Kármán model and devises an efficient energy decreasing iterative scheme.

1. INTRODUCTION

Föppl–von Kármán models have recently attracted attention among applied mathematicians due to their capability of describing various nonlinear effects in the elastic deformation of thin elastic objects. These effects are important in the development of various applications including nanotechnologies, cf., e.g., [JC04]. The most common model describes the moderate deformation of a plate $\omega \subset \mathbb{R}^2$ with thickness $\gamma > 0$ via an in-plane displacement $u : \omega \to \mathbb{R}^2$ and a deflection $w : \omega \to \mathbb{R}$ that minimize the dimensionally reduced elastic energy functional

$$E(u,w) = \frac{\gamma^2}{2} \int_\omega |D^2 w|^2 \,\mathrm{d}x + \frac{1}{2} \int_\omega |\widetilde{\varepsilon}(u) + \nabla w \otimes \nabla w|^2 \,\mathrm{d}x - \int_\omega f w \,\mathrm{d}x$$

in a set of admissible pairs contained in the product space $H^1(\omega;\mathbb{R}^2) \times H^2(\omega)$ incorporating appropriate boundary conditions. The functional E involves a vertical dead body load $f : \omega \to \mathbb{R}$, twice the symmetric gradient $\widetilde{\varepsilon}(u) = Du + Du^\top$, and the dyadic product $a \otimes b = ab^\top$ of the deflection gradient. Norms and inner products of vectors or matrices are defined via euclidean length and Frobenius norm, respectively. The model results from a simplification of three-dimensional hyperelastic material descriptions and we refer the reader to [Cia80, Cia97, FJM02, FJM06] for related details.

Thin elastic sheets display a rich variety of nonlinear effects depending, e.g., on relations between geometry, thickness, applied forces, and boundary conditions. Mathematically this results in a continuum of combinations of bending and membrane phenomena. Important special cases can be identified via a particular scaling of the energy in terms of the thickness parameter

Date: April 8, 2016.

γ, cf. [FJM06]. While pure membrane and bending models entirely eliminate the parameter γ, the Föppl–von Kármán model considered here includes it and thereby incorporates a length scale that determines the geometry of folding patterns and ridges, cf., e.g., [MO14, Ven04]. The occurrence of these phenomena can be understood by comparing the elastic energy functional to functionals arising in phase field models or mathematical descriptions of crystalline phase transitions, cf. [KM94, DHR16]. The combination of a higher order term weighted by a small factor with a nonconvex term specifying certain prefered states leads to the formation of interfaces or branching structures. Qualitatively, minimizers can in idealized situations be precisely characterized via optimal energy scaling laws in terms of γ and other relevant quantities, cf. [CM08, BK14, COT15]

Due to the nonconvex and singularly perturbed character of the elastic energy functional and the corresponding complicated structure of energy minimizing displacements it is difficult to numerically compute global minimizers. The author is unaware of articles discussing the discretization and iterative solution of the Föppl–von Kármán model except for the article [CGK07] in which convergence is investigated in an abstract framework. To detect stationary configurations with low elastic energy we employ a discrete gradient flow for E with respect to the variables u and w, i.e., the coupled system of nonlinear evolution equations

$$\begin{aligned}\big(\partial_t w, v\big)_{ver} &= -\partial_w E(u,w)[v]\\ &= -\gamma^2\big(D^2 w, D^2 v\big) - 2\big(|\nabla w|^2\nabla w + \widetilde{\varepsilon}(u)\nabla w, \nabla v\big) + \big(f, v\big),\\ \big(\partial_t u, z\big)_{hor} &= -\partial_u E(u,w)[z]\\ &= -\big(\widetilde{\varepsilon}(u), \widetilde{\varepsilon}(z)\big) - \big(\nabla w\otimes\nabla w, \widetilde{\varepsilon}(z)\big),\end{aligned}$$

where $\partial_w E$ and $\partial_u E$ denote the Fréchet derivatives of E with respect to w and u while $(\cdot,\cdot)_{ver}$ and $(\cdot,\cdot)_{hor}$ are inner products on $H^2(\omega)$ and $H^1(\omega;\mathbb{R}^2)$, respectively. The L^2 inner product is denoted by $(\cdot,\cdot)$ with corresponding norm $\|\cdot\|$; we used that $|a\otimes a|^2 = |a|^4$ and $M : (a\otimes b) = (Ma)\cdot b = (Mb)\cdot a$ for every symmetric matrix $M\in\mathbb{R}^{2\times 2}$ and all $a, b\in\mathbb{R}^2$.

To discretize the evolution equations we choose a sequence of positive step sizes $(\tau_k)_{k=1,2,\dots}$ and replace time derivatives by the backward difference quotients

$$d_t u^k = \frac{1}{\tau_k}\big(u^k - u^{k-1}\big), \quad d_t w^k = \frac{1}{\tau_k}\big(w^k - w^{k-1}\big).$$

A fully implicit discretization of the right-hand sides would lead to a coupled system of nonlinear equations which might be difficult to solve while a fully explicit discretization leads to restrictive conditions to ensure stability. To decouple the equations and obtain equations that can be solved efficiently we exploit the special structure of the nonlinearity and make use of the delay effect of the discrete product rule. This leads to the following iterative

scheme: given (u^{k-1}, w^{k-1}) compute (u^k, w^k) such that

$$\begin{aligned}\big(d_t w^k, v\big)_{ver} &= -\gamma^2\big(D^2 w^k, D^2 v\big) \\ &\quad - 2\big(|\nabla w^k|^2 \nabla w^k + \widetilde{\varepsilon}(u^{k-1})\nabla w^{k-1/2}, \nabla v\big) + \big(f, v\big), \\ \big(d_t u^k, z\big)_{hor} &= -\big(\widetilde{\varepsilon}(u^k), \widetilde{\varepsilon}(z)\big) - \big(\nabla w^k \otimes \nabla w^k, \widetilde{\varepsilon}(z)\big),\end{aligned}$$

for all (v, z) satisfying homogeneous boundary conditions. The scheme involves the average $w^{k-1/2}$ defined for w^k and w^{k-1} by

$$w^{k-1/2} = \frac{1}{2}\big(w^k + w^{k-1}\big).$$

Note that the equations defining w^k and u^k are decoupled in the sense that the equation for w^k does not involve u^k. By testing the discrete evolution system with (u^k, w^k) we see that the scheme is unconditionally stable and energy decreasing. Moreover, it follows that the iteration converges to a stationary pair (u, w). Well posedness of the equations is a consequence of the fact that they define optimality conditions for strongly convex minimization problems under a mild condition on τ_k. In particular, the Newton iteration is expected to have good convergence properties in the iterative solution of the equation for w^k, whereas the equation defining u^k is a linear problem with coercive and symmetric bilinear form. The unconditional stability of the discrete gradient flow allows us to use arbitrary step sizes $\tau_k > 0$ but too large steps might lead to nonuniquness and divergence of the Newton iteration. To obtain an efficient and stable scheme we use the following adaptive strategy to adjust the step size:

- decrease τ_k until Newton scheme terminates within L iterations
- set $\tau_{k+1} = \min\{2\tau_k, 10^r\}$ for next gradient flow step

Here r is an appropriate positive integer to avoid numerical overflow. Since the Newton scheme always converges under a mild condition on τ_k, the algorithm converges to a stationary configuration. The use of variable step sizes turns out to be particularly useful to avoid local minimizers.
The spatial discretization of the Föppl–von Kármán model is based on standard $P1$ finite elements for the in-plane displacement and Kirchhoff triangles for the deflection. The latter element defines a nonconforming bending element whose degrees of freedom are the deflections and their gradients at the nodes of a triangulation which coincide with the vertices of triangles. This element has recently been used in the closely related problem of computing bending isometries [Bar13, Bar15, BBN15]. The fact that the gradient values are explicit degrees of freedom allows for a practical discretization of nonlinear terms making appropriate use of numerical integration and direct incorporation of a large class of boundary conditions. In particular, our

discretization of the elastic energy is given by

$$E_h(u_h,w_h)=\frac{\gamma}{2}\int_\omega|\nabla\nabla_h w_h|^2\,\mathrm{d}x + \frac{1}{2}\int_\omega\widehat{\mathcal{I}}_h\big[|\widetilde{\varepsilon}(u_h)+\nabla w_h\otimes\nabla w_h|^2\big]\,\mathrm{d}x-\int_\omega\widehat{\mathcal{I}}_h[fw_h]\,\mathrm{d}x.$$

Here ∇_h is a discrte gradient operator whose image belongs to $H^1(\omega;\mathbb{R}^2)$ and $\widehat{\mathcal{I}}_h$ is the elementwise nodal interpolant related to a regular triangulation which extends the standard nodal interpolant to elementwise continuous functions. We show that the energies E_h converge to E in the sense of Γ-convergence in $H^1(\omega;\mathbb{R}^2)\times W^{1,4}(\omega)$ with respect to the weak convergence in $H^1(\omega;\mathbb{R}^2)$ and strong convergence in $W^{1,4}(\omega)$. In fact we have that the discrete Hessians $\nabla\nabla_h w_h$ converge weakly in $L^2(\omega;\mathbb{R}^{2\times2})$. The minimization of E_h is done with a corresponding discretization of the discrete gradient flow described above. The complete justification of our numerical method thus leaves a gap in that Γ-convergence implies convergence of almost global minimizers for E_h to global minimizers for E while the gradient flow can in general only be expected to detect local minimizers. For a discussion of the approximation of local minimizers and evolutions within the framework of Γ-convergence we refer the reader to [Bra14].

We discuss the practical performance of our numerical method by considering various practically motivated settings including the indentation of elastic cones and compression of thin elastic sheets. The results qualitatively confirm theoretical findings from [Bel15, BCM15, COT15]. Related experiments using a shell model have recently been reported in [NR14].

The outline of the article is as follows. In Section 2 we introduce relevant notation and define suitable finite element spaces. Section 3 is devoted to the unconditional stability analysis of the discretized gradient flow. In Section 4 we show that the spatial discretization converges in the sense of Γ-convergence to the continuous Föppl–von Kármán model. Various numerical experiments are reported in Section 5.

2. Preliminaries

II.A. **Mathematical model.** A rigorous justification of the Föppl–von Kármán model starts from three-dimensional hyperelasticity and the energy functional

$$E_{3d}(y)=\int_{\Omega_\gamma}W(\widehat{\nabla}y)\,\mathrm{d}\widehat{x}-\int_{\Omega_\gamma}\widehat{f}\cdot y\,\mathrm{d}\widehat{x},$$

where $\Omega_\gamma=\omega\times(-\gamma/2,\gamma/2)$ is a flat plate of thickness $\gamma>0$ and $W:\mathbb{R}^{3\times3}\to\mathbb{R}$ a stored energy function obeying physical requirements. Small energies are related to deformation gradients $\widehat{\nabla}y$ that are close to rotations and give rise to linearizing W about the identity matrix and considering the quadratic form

$$Q_3(F)=\frac{\partial^2W}{\partial F^2}(I)[F,F]$$

and a corresponding two-dimensional variant

$$Q_2(G) = \min_{a\in\mathbb{R}^3} Q_3(\widehat{G} + a\otimes e_3 + e_3\otimes a)$$

with the canonical basis vector $e_3 \in \mathbb{R}^3$ and the matrix $\widehat{G} \in \mathbb{R}^{3\times 3}$ obtained by augmenting $G \in \mathbb{R}^{2\times 2}$ with a trivial row and column. For isotropic materials one obtains

$$Q_2(G) = \frac{\mu}{2}|G + G^\top|^2 + \frac{2\mu\lambda}{2\mu+\lambda}(\operatorname{tr} G)^2$$

with the Lamé coefficients λ, μ. By an appropriate rescaling of $y : \Omega_\gamma \to \mathbb{R}^3$ and $f = \widehat{f_3} : \Omega_\gamma \to \mathbb{R}$ one obtains the Föppl–von Kármán functional

$$E^{FvK}(u,w) = \frac{1}{24}\int_\omega Q_2(D^2 w)\,\mathrm{d}x + \frac{1}{8}\int_\omega Q_2\big(\widetilde{\varepsilon}(u) + \nabla w\otimes\nabla w\big)\,\mathrm{d}x - \int_\omega f w\,\mathrm{d}x.$$

We refer the reader to [FJM06] for details but note that the reduced model can heuristically be obtained from the ansatz

$$y(x,x_3) = \begin{bmatrix} x + \gamma^2 u(x) - \gamma^2 x_3 \nabla w(x) \\ x_3 + w(x)\end{bmatrix}.$$

To capture a larger class of effects we consider the corresponding functional

$$E(u,w) = \frac{\gamma^2}{2}\int_\omega |D^2 w|^2\,\mathrm{d}x + \frac{1}{2}\int_\omega \big|\widetilde{\varepsilon}(u) + \nabla w\otimes\nabla w\big|^2\,\mathrm{d}x - \int_\omega f w\,\mathrm{d}x$$

which is a rescaled version of E^{FvK} for an isotropic material. The functional is defined on a set of admissible pairs, i.e., for

$$(u,w) \in \mathcal{A} = \mathcal{A}_0 + (u_{\mathrm{D}}, w_{\mathrm{D}}) \subset H^1(\omega;\mathbb{R}^2)\times H^2(\omega).$$

We assume that $\mathcal{A}$ is an affine subspace corresponding to a linear subspace $\mathcal{A}_0$ for which we have the Korn–Poincaré inequality

$$\|\widetilde{u}\|_{H^1(\omega)} + \|\widetilde{w}\|_{H^2(\omega)} \le c_P\big(\|\widetilde{\varepsilon}(\widetilde{u})\| + \|D^2\widetilde{w}\|\big) \tag{1}$$

for all $(\widetilde{u},\widetilde{w}) \in \mathcal{A}_0$. This is satisfied if, e.g., $\widetilde{u} = 0$ and $w = 0$ and $\nabla w = 0$ on a subset $\gamma_{\mathrm{D}} \subset \partial\omega$ of positive surface measure or if $\widetilde{u} = 0$ and $\widetilde{w} = 0$ on $\partial\omega$. We also assume that the boundary conditions are such that the we have the Sobolev inequality with seminorms

$$\|\nabla\widetilde{w}\|_{L^4(\omega)} \le c_S\|D^2\widetilde{w}\| \tag{2}$$

for all $\widetilde{w} \in \mathcal{A}_0$.

II.B. **Discrete time derivatives.** For a sequence of possibly nonuniform step sizes $(\tau_k)_{k=1,\dots,K}$ and a sequence $(a^k)_{k=0,\dots,K}$ we set

$$d_t a^k = \frac{1}{\tau_k}(a^k - a^{k-1}).$$

Note that binomial formulas imply the relations

$$\begin{aligned} 2d_t a^k \cdot a^k &= d_t|a^k|^2 + \tau_k|d_t a^k|^2, \\ 2d_t a^k \cdot a^{k-1/2} &= d_t|a^k|^2. \end{aligned}$$

We also recall the discrete product rule

$$d_t(a^k b^k) = (d_t a^k) b^k + a^{k-1}(d_t b^k)$$

valid for sequences $(a_k)_{k=0,\dots,K}$ and $(b_k)_{k=0,\dots,K}$.

II.C. $P1$ **finite element spaces.** For a regular triangulation $\mathcal{T}_h$ of the polygonal domain $\omega \subset \mathbb{R}^2$ into closed triangles $T \in \mathcal{T}_h$ of diameter $h_T = \operatorname{diam}(T)$ with $h_T \le ch$ we let

$$\mathcal{S}^1(\mathcal{T}_h) = \{v_h \in C(\overline{\omega}) : v_h|_T \text{ affine for all } T \in \mathcal{T}_h\}$$

denote the standard $P1$ finite element space. The nodal basis functions $(\varphi_z)_{z\in\mathcal{N}_h} \subset \mathcal{S}^1(\mathcal{T}_h)$ associated with the set of nodes $\mathcal{N}_h$ satisfy $\varphi_z(y) = \delta_{zy}$ for all $z, y \in \mathcal{N}_h$. We also use the space of discontinous $P1$ functions defined via

$$\widehat{\mathcal{S}}^1(\mathcal{T}_h) = \{v_h \in L^\infty(\omega) : v_h|_T \text{ affine for all } T \in \mathcal{T}_h\}.$$

The elementwise nodal interpolant $\widehat{\mathcal{I}}_h v \in \widehat{\mathcal{S}}^1(\mathcal{T}_h)$ of a function $v \in L^\infty(\omega)$ with $v|_T \in C(T)$ for all $T \in \mathcal{T}_h$ defines a linear operator via

$$\widehat{\mathcal{I}}_h v = \sum_{T\in\mathcal{T}_h} \sum_{z\in\mathcal{N}_h\cap T} v|_T(z)\varphi_z|_T.$$

Here $\varphi_z|_T \in L^\infty(\omega)$ is the discontinuous function that coincides with φ_z on T and is zero in $\omega \setminus T$. If $v \in C(\overline{\omega})$ then $\widehat{\mathcal{I}}_h v \in \mathcal{S}^1(\mathcal{T}_h)$ is the standard nodal interpolant of v. The L^2 inner product is approximated via

$$(v, w)_h = \int_\omega \widehat{\mathcal{I}}_h[v \cdot w]\,\mathrm{d}x = \sum_{T\in\mathcal{T}_h} \sum_{z\in\mathcal{N}_h\cap T} \beta_z^T v|_T(z) \cdot w|_T(z)$$

for elementwise continuous functions or vector fields $v, w \in L^\infty(\overline{\omega}; \mathbb{R}^\ell)$, where

$$\beta_z^T = \int_T \varphi_z \,\mathrm{d}x$$

for all $T \in \mathcal{T}_h$ and $z \in \mathcal{N}_h \cap T$. We define the space of continuous $P1$ vector fields on ω via

$$V_h = \mathcal{S}^1(\mathcal{T}_h)^2.$$

II.D. **Kirchhoff elements.** For an integer $r \ge 0$ we let $\mathcal{P}_r(T)$ be the set of polynomials of total degree at most r on $T \in \mathcal{T}_h$ and, if $z_1, z_2, z_3 \in \mathcal{N}_h \cap T$ are the vertices of T and $x_T = (z_1 + z_2 + z_3)/3$,

$$\mathcal{P}_{3,\mathrm{red}}(T) = \big\{p \in \mathcal{P}_3(T) : p(x_T) = \frac{1}{3}\sum_{j=1}^3 \big[p(z_j) + \nabla p(z_j) \cdot (x_T - z_j)\big]\big\},$$

where the constraint excludes the subspace of functions satisfying $p(z_j) = 0$ and $\nabla p(z_j) = 0$ for $j = 1, 2, 3$ so that these quantities define the remaining

nine degrees of freedom. We then set

$$W_h = \big\{ w_h \in C(\overline{\omega}) : w_h|_T \in \mathcal{P}_{3,\mathrm{red}}(T) \text{ for all } T \in \mathcal{T}_h \\ \text{and } \nabla w_h \text{ is continuous in } \mathcal{N}_h \big\},$$
$$Z_h = \big\{ \theta_h \in C(\overline{\omega}; \mathbb{R}^2) : \theta_h|_T \in \mathcal{P}_2(T)^2 \big\}.$$

Recall that the degrees of freedom in $\mathcal{P}_2(T)$ are the function values at the vertices and at the midpoint of edges of T, cf. Figure 1. We define a discrete gradient operator

$$\nabla_h : W_h \to Z_h$$

for $w_h \in W_h$ by the conditions that for $\psi_h = \nabla_h w_h \in Z_h$ we have

$$\psi_h(z) = \nabla w_h(z)$$

for all $z \in \mathcal{N}_h$ and

$$\psi_h(z_E) = \frac{1}{2}\big[\big(\nabla w_h(z_1) + \nabla w_h(z_2)\big) \cdot n_E\big] n_E + \big[\nabla w_h(z_E) \cdot t_E\big] t_E$$

for every edge $E \subset \partial T$ with endpoints $z_1, z_2 \in \mathcal{N}_h \cap E$, midpoint z_E, and with $n_E, t_E \in \mathbb{R}^2$ denoting two orthogonal unit vectors such that n_E is perpendicular to E. In particular, the quadratic function $\nabla_h w_h$ has a linear normal component along the edges of T. The mapping ∇_h and the finite element spaces are schematically sketched in Figure 1 and can naturally be extended to functions in $H^3(\Omega) \subset C^1(\overline{\Omega})$, i.e., given $w \in H^3(\omega)$ we define $\psi_h = \nabla_h w \in Z_h$ by the six conditions above.

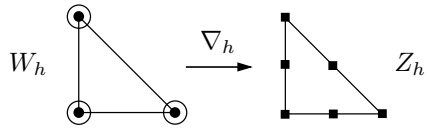

FIGURE 1. Schematic description of the discrete gradient operator $\nabla_h : W_h \to V_h$ and degrees of freedom of the polynomial spaces $\mathcal{P}_{3,\mathrm{red}}$ and $[\mathcal{P}_2]^2$.

Lemma II.1 (Properties of ∇_h, [Bra07, BBN15])**.** *(i) There exist $c_1, c_2 > 0$ such that for all $w_h \in W_h$ and $T \in \mathcal{T}_h$ we have for $\ell = 0, 1$ that*

$$c_1^{-1} \|\nabla^{\ell+1} w_h\|_{L^2(T)} \le \|\nabla^\ell \nabla_h w_h\|_{L^2(T)} \le c_1 \|\nabla^{\ell+1} w_h\|_{L^2(T)},$$

and for $2 \le p \le \infty$

$$\|\nabla_h w_h - \nabla w_h\|_{L^p(T)} \le c_2 h_T \|D^2 w_h\|_{L^p(T)}.$$

(ii) There exists $c_3 > 0$ such that for all $w \in H^3(\Omega)$ and $T \in \mathcal{T}_h$ we have

$$\|\nabla_h w - \nabla w\|_{L^2(T)} + h_T \|\nabla \nabla_h w - D^2 w\|_{L^2(T)} \le c_3 h_T^2 \|w\|_{H^3(T)}.$$

(iii) The mapping $w_h \mapsto \|\nabla\nabla_h w_h\|$ defines a norm on the sets

$$W_{0,h}^{simple} = \big\{w_h \in W_h : w_h(z) = 0,\ \nabla w_h(z) = 0 \text{ for all } z \in \mathcal{N}_h \cap \gamma_{\mathrm{D}}\big\},$$
$$W_{0,h}^{supp} = \big\{w_h \in W_h : w_h(z) = 0 \text{ for all } z \in \mathcal{N}_h \cap \partial\omega\big\}.$$

Proof. The estimates follow from linearity of the mapping $w_h \mapsto \nabla_h w_h$, injectivity of $\nabla w_h \mapsto \nabla_h w_h$, the Bramble-Hilbert lemma, and transformation arguments, cf. [Bra07, BBN15] for details. □

3. Energy decreasing iteration

III.A. **Energy decay.** We analyze in this section the discrete gradient flow assuming for simplicity that $f = 0$.

Algorithm III.1 (Decoupled gradient flow)**.** *Choose $(u^0, w^0) \in \mathcal{A}$, an initial step size $\tau_1 > 0$, and a stopping criterion $\varepsilon_{stop} > 0$, and set $k = 1$.*
(1) Compute $(u^k, w^k) \in \mathcal{A}$ such that

$$\big(d_t w^k, v\big)_{ver} = -\gamma^2\big(D^2 w^k, D^2 v\big) - 2\big(|\nabla w^k|^2 \nabla w^k + \widetilde{\varepsilon}(u^{k-1})\nabla w^{k-1/2}, \nabla v\big),$$
$$\big(d_t u^k, z\big)_{hor} = -\big(\widetilde{\varepsilon}(u^k), \widetilde{\varepsilon}(z)\big) - \big(\nabla w^k \otimes \nabla w^k, \widetilde{\varepsilon}(z)\big),$$

for all $(z, v) \in \mathcal{A}_0$.
(2) Stop if $\|d_t w^k\|_{ver} + \|d_t u^k\|_{hor} \le \varepsilon_{stop} \min\{1, \tau_k\}$; define $\tau_{k+1} > 0$, increase $k \to k+1$, and continue with (1) otherwise.

The iteration is well-posed, unconditionally stable, and energy decreasing.

Proposition III.2. *Algorithm III.1 admits iterates $(u^k, w^k)_{k=0,1,\dots} \subset \mathcal{A}$ which satisfy*

$$E(u^K, w^K) + \sum_{k=1}^{K} \tau_k\big(\|d_t w^k\|_{ver}^2 + \|d_t u^k\|_{hor}^2\big) \le E(u^0, w^0).$$

In particular, $(d_t u^k, d_t w^k) \to 0$ and every cluster point of the sequence $(u^k, w^k)_{k=0,1,\dots}$ is a stationary point for E. The iterates are unique if we have $\|D^2 \cdot\| \le c_{eq}\|\cdot\|_{ver}$ and

$$\tau_k \le \frac{1}{2c_0 c_{eq} c_S^2}$$

for $k = 1, 2, \dots$ with a constant c_0 depending on γ, c_S, w_{D}, and $E(u_0, w_0)$.

Proof. Note that given w^k the equation specifying u^k defines a linear problem which by Lax–Milgram lemma admits a unique solution. The equation defining w^k is the optimality condition for the minimization problem:

$$\begin{aligned}\text{Minimize } w \mapsto & \frac{1}{2\tau_k}\|w - w^{k-1}\|_{ver}^2 + \frac{\gamma^2}{2}\|D^2 w\|^2 + \frac{1}{2}\int_\omega |\nabla w|^4 \,\mathrm{d}x \\ & + \frac{1}{2}\int_\Omega \widetilde{\varepsilon}(u^{k-1}) : \big(\nabla[w + w^{k-1}] \otimes \nabla[w + w^{k-1}]\big)\,\mathrm{d}x.\end{aligned} \tag{3}$$

Lower semicontinuity and coercivity on $H^2(\omega)$ imply the existence of a minimizer w^k. We test the first equation of the iterative scheme with $v = d_t w^k$ and the second one with $z = d_t u^k$. The discrete product rule and the binomial formulas from Subsection II.B imply that we have

$$2\big(\widetilde{\varepsilon}(u^{k-1})\nabla w^{k-1/2}, \nabla d_t w^k\big) + \big(\nabla w^k \otimes \nabla w^k, \widetilde{\varepsilon}(d_t u^k)\big) = d_t\big(\widetilde{\varepsilon}(u^k), \nabla w^k \otimes \nabla w^k\big).$$

Incorporating convexity of $|\nabla w|^4$, we find after summation of the discrete evolution equations that

$$\begin{aligned}
\|d_t w^k\|_{ver}^2 + \frac{\gamma^2}{2}\big(d_t\|D^2 w^k\|^2 + \tau\|D^2 d_t w^k\|^2\big) \\
+ \|d_t u^k\|_{hor}^2 + \frac{1}{2}\big(d_t\|\widetilde{\varepsilon}(u^k)\|^2 + \tau\|\widetilde{\varepsilon}(d_t u^k)\|^2\big) \\
= -2\big(\widetilde{\varepsilon}(u^{k-1})\nabla w^{k-1/2}, \nabla d_t w^k\big) - \big(\nabla w^k \otimes \nabla w^k, \widetilde{\varepsilon}(d_t u^k)\big) \\
- 2\big(|\nabla w^k|^2 \nabla w^k, \nabla d_t w^k\big) \\
\le -d_t\big(\widetilde{\varepsilon}(u^k), \nabla w^k \otimes \nabla w^k\big) - \frac{d_t}{2}\int_\omega |\nabla w^k|^4 \,\mathrm{d}x.
\end{aligned}$$

A summation over $k = 1, 2, \dots, K$ proves the asserted estimate which then implies that $\gamma^2\|D^2 w^k\|^2 \le E_0 = E(u_0, w_0)$ for $k = 0, 1, \dots, K$. Together with the Sobolev inequality (2) we obtain the estimate

$$\begin{aligned}
\|\widetilde{\varepsilon}(u^k)\| &\le \|\widetilde{\varepsilon}(u^k) + \nabla w^k \otimes \nabla w^k\| + \|\nabla w^k\|_{L^4(\omega)}^2 \\
&\le E_0^{1/2} + 2\|\nabla w_{\mathrm{D}}\|_{L^4(\omega)}^2 + 2\|\nabla(w^k - w_{\mathrm{D}})\|_{L^4(\omega)}^2 \\
&\le E_0^{1/2} + 2\|\nabla w_{\mathrm{D}}\|_{L^4(\omega)}^2 + 2c_S^2\|D^2(w^k - w_{\mathrm{D}})\|^2,
\end{aligned}$$

i.e., $\|\widetilde{\varepsilon}(u^k)\| \le c_0$, $k = 0, 1, \dots, K$. This estimate leads to

$$\begin{aligned}
\frac{1}{2}\int_\omega \widetilde{\varepsilon}(u^{k-1}) : \nabla w \otimes \nabla w \,\mathrm{d}x &\ge -\frac{1}{2}\|\widetilde{\varepsilon}(u^{k-1})\|\|\nabla w\|_{L^4(\omega)}^2 \\
&\ge -\|\widetilde{\varepsilon}(u^{k-1})\|\|\nabla(w - w^{k-1})\|_{L^4(\omega)}^2 - \|\widetilde{\varepsilon}(u^{k-1})\|\|\nabla w^{k-1}\|_{L^4(\omega)}^2 \\
&\ge -c_0 c_S^2\|D^2(w - w^{k-1})\|^2 - \|\widetilde{\varepsilon}(u^{k-1})\|\|\nabla w^{k-1}\|_{L^4(\omega)}^2.
\end{aligned}$$

This implies strong convexity of the minimization problem (3) and thus uniqueness of the minimizer w^k provided that $\tau_k \le 1/(2c_0 c_{eq} c_S^2)$. □

III.B. **Newton iteration.** The first step of Algorithm III.1 defines a nonlinear system of equations, i.e., we seek $w^k \in W$ such that $F(w^k)[v] = 0$ for all $v \in W$, where with $\widehat{w} = w^{k-1}$ and $\widehat{Z} = \widetilde{\varepsilon}(u^{k-1})/2$ and $\tau = \tau_k$ we have

$$\begin{aligned}
F(w)[v] = (D^2[w - \widehat{w}], D^2 v) + \gamma^2\tau(D^2 w, D^2 v) \\
+ 2\tau\big(\big[|\nabla w|^2 + \widehat{Z}\big]\nabla w + \widehat{Z}\nabla\widehat{w}, \nabla v\big),
\end{aligned}$$

We assumed for simplicity that the scalar product related to the seminorm is given by $\|\cdot\|_{ver} = \|D^2\cdot\|$. The Fréchet derivative of F is given by

$$F'(w)[v,y] = (1+\gamma^2\tau)(D^2y, D^2v) + 2\tau\big(\big[2\nabla w\otimes\nabla w + |\nabla w|^2 + \widehat{Z}\big]\nabla y, \nabla v\big).$$

Proposition III.2 implies that the equation $F(w)[v]=0$ admits a unique solution $w\in W$ if $\tau\le c'$. Since

$$F'(w)[v,v] \ge (1+\gamma^2\tau)\|D^2v\|^2 - 2\tau\big\|2\nabla w\otimes\nabla w + |\nabla w|^2 I_2 + \widehat{Z}\big\|\|\nabla v\|_{L^4(\omega)}^2$$

it follows that the bilinear form $F'(w)$ is uniformly coercive if $\tau\le c''$. Hence, noting appropriate continuity properties of F and F' we have that the Newton iteration for the solution of $F(w)[v]=0$ converges quadratically provided that $\tau\le c'''$ for a some constant $c'''>0$.

4. Discretization and Γ-convergence

We define a discretization of E via

$$E_h(u_h,w_h) = \frac{\gamma^2}{2}\int_\omega |\nabla\nabla_h w_h|^2\,\mathrm{d}x + \frac{1}{2}\int_\omega \widehat{\mathcal{I}}_h|\widetilde{\varepsilon}(u_h)+\nabla w_h\otimes\nabla w_h|^2\,\mathrm{d}x$$

for $(u_h,w_h)\in V_h\times W_h$, where we omit for simplicity the forcing term defined by f. The functionals E_h approximate E in the sense of Γ-convergence for a sequence of triangulations $(\mathcal{T}_h)_{h>0}$ with $h\to 0$.

Theorem IV.1 (Γ-convergence)**.** *(i) Assume that $(u_h,w_h)_{h>0}$ is a sequence with $(u_h,w_h)\in V_h\times W_h$ and*

$$E_h(u_h,w_h) + \|w_h\|_{W^{1,4}(\omega)} + \|u_h\|_{H^1(\omega;\mathbb{R}^2)} \le c \tag{4}$$

for all $h>0$. For every weak accumulation point $(u,w)\in H^1(\omega;\mathbb{R}^2)\times W^{1,4}(\omega)$ we have $w\in H^2(\omega)$, $w_{h'}\to w$ strongly in $W^{1,4}(\omega)$ for a subsequence $(w_{h'})_{h'>0}$, and

$$E(u,w)\le\liminf_{h\to 0} E_h(u_h,w_h).$$

(ii) For every $(u,w)\in H^1(\omega;\mathbb{R}^2)\times H^2(\omega)$ there exists a sequence $(u_h,w_h)_{h>0}$ such that $(u_h,w_h)\in V_h\times W_h$ for all $h>0$,

$$(u_h,w_h)\to(u,w)\quad \text{in } H^1(\omega;\mathbb{R}^2)\times W^{1,4}(\omega)$$

as $h\to 0$, and

$$\lim_{h\to 0} E_h(u_h,w_h) = E(u,w).$$

Proof. We first control the influence of numerical integration in E_h. We abbreviate $\psi_h = \widetilde{\varepsilon}(u_h)+\nabla w_h\otimes\nabla w_h$ and note that by elementwise nodal

interpolation and inverse estimates we have that

$$\Big|\int_\omega \widehat{\mathcal{I}}_h|\psi_h|^2\,\mathrm{d}x - \int_\omega |\psi_h|^2\,\mathrm{d}x\Big| \le c\sum_{T\in\mathcal{T}_h} h_T\big\|D|\psi_h|^2\big\|_{L^1(T)}$$
$$\le 2ch^{1/2}\big\|\widetilde{\varepsilon}(u_h)+\nabla w_h\otimes\nabla w_h\big\|\Big(\sum_{T\in\mathcal{T}_h} h_T\|\nabla w_h\|^2_{L^\infty(T)}\|D^2 w_h\|^2_{L^2(T)}\Big)^{1/2}.$$

With the inverse estimate $\|\nabla w_h\|_{L^\infty(T)} \le ch_T^{-1/2}\|\nabla w_h\|_{L^4(T)}$ we observe that the right-hand side tends to zero as $h\to 0$ provided that (4) holds.
(i) If $(u_h,w_h)_{h>0}$ is a sequence of finite element functions satisfying (4) then we have $\|\nabla\nabla_h w_h\|\le c$ and hence for some $Y\in H^1(\omega;\mathbb{R}^2)$ and $w\in W^{1,4}(\omega)$ after passage to subsequences that

$$\nabla_h w_h \rightharpoonup Y \text{ in } H^1(\omega;\mathbb{R}^2),$$
$$w_h \rightharpoonup w \text{ in } W^{1,4}(\omega),$$
$$\nabla_h w_h - \nabla w_h \to 0 \text{ in } L^4(\omega;\mathbb{R}^2),$$

where we also used that by Lemma II.1 and an inverse estimate we have

$$\|\nabla_h w_h - \nabla w_h\|_{L^4(\omega)} \le ch^{1/2}\|\nabla\nabla_h w_h\|_{L^2(\omega)}.$$

By uniqueness of weak limits we have that $\nabla w = Y$ and in particular that $w\in H^2(\omega)$. Note that $\nabla_h w_h \to Y = \nabla w$ in $L^4(\omega;\mathbb{R}^2)$ and hence also $\nabla w_h\to\nabla w$ in $L^4(\omega;\mathbb{R}^2)$. To deduce the asserted bound for $E(u,w)$ we note that due to the above control of numerical integratino we may equivalently consider the functionals

$$\widetilde{E}_h(u_h,w_h) = \frac{\gamma^2}{2}\int_\omega |\nabla\nabla_h w_h|^2\,\mathrm{d}x$$
$$+\frac12\int_\omega|\widetilde{\varepsilon}(u_h)|^2\,\mathrm{d}x + \int_\omega \widetilde{\varepsilon}(u_h):\nabla w_h\otimes\nabla w_h\,\mathrm{d}x + \frac12\int_\omega|\nabla w_h|^4\,\mathrm{d}x$$

instead of E_h. Weak lower semicontinuity of the convex terms and strong convergence of ∇w_h in $L^4(\omega;\mathbb{R}^2)$ then lead to the estimate.
(ii) By density of smooth functions and continuity properties of E we may assume that $(u,w)\in H^2(\omega;\mathbb{R}^2)\times H^3(\omega)$. We then let $u_h = \mathcal{I}_h u\in V_h$ and $w_h = \mathcal{I}_h^{3,\mathrm{red}} w\in W_h$ be the interpolants in the respective spaces. Interpolation estimates imply the asserted statement. □

Compactness, i.e., boundedness of the iterates in appropriate norms follows from appropriate boundary conditions as specified above for $\mathcal{A}_0$. We assume that strongly convergent approximations of the boundary data $(u_\mathrm{D},w_\mathrm{D})$ are given.

Proposition IV.2 (Compactness)**.** *Let (u_h,w_h) be a sequence with $(u_h,w_h)\in V_h\times W_h$ such that*

$$u_h = u_{\mathrm{D},h} + u_h',\quad w_h = w_{\mathrm{D},h} + w_h'$$

with functions $u_{\mathrm{D},h}, u_h' \in V_h$ *and* $w_{\mathrm{D},h}, w_h' \in W_h$ *such that*

$$u_{\mathrm{D},h} \to u_{\mathrm{D}} \text{ in } H^1(\omega;\mathbb{R}^2), \quad w_{\mathrm{D},h} \to w_{\mathrm{D}} \text{ in } W^{1,4}(\omega)$$

as $h \to 0$ *and*

$$u_h'|_{\gamma_{\mathrm{D}}} = 0, \quad w_h'|_{\gamma_{\mathrm{D}}} = 0, \quad \nabla w_h'|_{\gamma_{\mathrm{D}}} = 0$$

or

$$u_h'|_{\partial\omega} = 0, \quad w_h'|_{\partial\omega} = 0$$

for all $h > 0$*. Then, if* $E_h(u_h, w_h) \le c$ *for all* $h > 0$ *we have that*

$$\|u_h\|_{H^1(\omega;\mathbb{R}^2)} + \|w_h\|_{W^{1,4}(\omega)} \le c.$$

Proof. Boundedness of the discrete energies implies that $\nabla_h w_h$ is bounded in $H^1(\omega;\mathbb{R}^2)$ and since $\|\nabla\nabla_h \cdot\|$ defines a norm on functions in W_h satisfying the indicated homogeneous boundary conditions, we have that w_h is bounded in $W^{1,4}(\omega;\mathbb{R}^2)$. The same is true for ∇w_h. This implies that $\widetilde{\varepsilon}(u_h)$ is bounded in $L^2(\omega;\mathbb{R}^{2\times 2})$ and the boundary conditions together with Korn's inequality (1) yield that we have boundedness of $(u_h)_{h>0}$ in $H^1(\omega;\mathbb{R}^2)$. □

5. Numerical experiments

We apply in this section the numerical methods developed in the previous sections to different specifications of the nonlinearly elastic problem. We consider the discretized energy

$$\begin{aligned} E_h(u_h, w_h) =& \frac{\gamma^2}{2}\int_\omega |\nabla\nabla_h w_h|^2\,\mathrm{d}x + \frac{1}{2}\int_\omega \widehat{\mathcal{I}}_h|\widetilde{\varepsilon}(u_h) + \nabla w_h \otimes \nabla w_h|^2\,\mathrm{d}x \\ &- \int_\omega \widehat{\mathcal{I}}_h[f w_h]\,\mathrm{d}x - \int_\omega \widehat{\mathcal{I}}_h[g\cdot u_h]\,\mathrm{d}x \end{aligned}$$

in which we included an artificial horizontal forcing term defined by a vector field g. The stability analysis from Section 3 for the discrete gradient flow in the case of the continuous energy functional carries over to the discretized functional and we apply it to detect stationary configurations of low energy for E_h. We let

$$\mathcal{A}_{0,h} = V_{0,h} \times W_{0,h}$$

be a linear space incorporating homogeneous boundary conditions specified in the examples below and set

$$\mathcal{A}_h = (u_{\mathrm{D},h}, w_{\mathrm{D},h}) + \mathcal{A}_{0,h}$$

for approximations $u_{\mathrm{D},h} \in V_h$ and $w_{\mathrm{D},h} \in W_h$ of the exact boundary data functions. We abbreviate the discrete Hessian matrix for $w_h \in W_h$ by

$$D_h^2 w_h = \nabla\nabla_h w_h.$$

The discrete gradient flow is defined using the inner products

$$(w_h, v_h)_{ver} = \big(D_h^2\cdot, D_h^2 v_h\big), \quad (u_h, z_h)_{hor} = \big(\widetilde{\varepsilon}(u_h), \widetilde{\varepsilon}(z_h)\big)$$

for $w_h, v_h \in W_h$ and $u_h, z_h \in V_h$, respectively. With this, the fully discrete iterative scheme reads as follows.

Algorithm V.1 (Discrete decoupled gradient flow)**.** *Choose* $(u_h^0, w_h^0) \in \mathcal{A}_h$*, a prescribed maximal number of Newton iterations* $L > 0$*, stopping tolerances* $\varepsilon_{stop}, \varepsilon_{Newton} > 0$*, and an initial step size* $\tau_1 > 0$*, set* $k = 1$*.*
(1a) Repeatedly decrease τ_k *until the Newton scheme terminates within* L *steps and tolerance* ε_{Newton} *to determine* $w_h^k \in w_{\mathrm{D},h} + W_{0,h}$ *such that*

$$\begin{aligned}\big(D_h^2 d_t w_h^k, D_h^2 v_h\big) &= -\gamma^2\big(D_h^2 w_h^k, D_h^2 v_h\big)\\ &\quad - 2\big(|\nabla w_h^k|^2 \nabla w_h^k + \widetilde{\varepsilon}(u_h^{k-1})\nabla w_h^{k-1/2}, \nabla v_h\big)_h + \big(f, w_h\big)_h.\end{aligned}$$

for all $v_h \in W_h$*.*
(1b) Compute $u_h^k \in u_{\mathrm{D},h} + V_{0,h}$ *such that*

$$\big(d_t\widetilde{\varepsilon}(u_h^k), \widetilde{\varepsilon}(z_h)\big) = -\big(\widetilde{\varepsilon}(u_h^k), \widetilde{\varepsilon}(z_h)\big) - \big(\nabla w_h^k \otimes \nabla w_h^k, \widetilde{\varepsilon}(z_h)\big)_h + \big(g, z_h\big)_h$$

for all $z_h \in V_{0,h}$*.*
(2) Stop if $\|d_t D_h^2 w_h^k\| + \|d_t\widetilde{\varepsilon}(u_h^k)\| \le \varepsilon_{stop}\min\{1, \tau_k\}$*; define*

$$\tau_{k+1} = \min\big\{2\tau_k, 10^r\big\},$$

increase $k \to k+1$*, and continue with (1) otherwise.*

Unless otherwise stated we use the stopping criterion $\varepsilon_{stop} = h/10$; we terminate the Newton iteration once the correction $c_h \in W_h^0$ satisfies $\|D_h^2 c_h\| \le \varepsilon_{Newton} = 10^{-5}$ and choose $L = 5$ as the maximal number of iterations. This leads to a neglible error contribution for the employed mesh sizes in the range $h \in [10^{-4}, 10^{-2}]$. The maximal step size was set to $\tau_{max} = 10^5$, i.e., $r = 5$. The total CPU time of Algorithm V.1 in the experiments reported below was on the order of a few minutes for $h \sim 10^{-2}$ and hours for $h \sim 10^{-4}$ for our straightforward Matlab implementation run on a standard desktop.

V.A. **Experimental convergence rate.** To determine an experimental convergence rate for our numerical method we consider a square plate that is clamped on one side. To identify a reference solution, we consider an additional, artificial forcing field g in the equation for u, i.e., we prescribe functions (u, w) and compute (f, g) such that

$$\begin{aligned}\gamma^2\Delta^2 w - 2\,\mathrm{div}\,\big(\big[|\nabla w|^2 + \widetilde{\varepsilon}(u)\big]\nabla w\big) &= f,\\ -2\,\mathrm{div}\,\big(\widetilde{\varepsilon}(u) + \nabla w \otimes \nabla w\big) &= g,\end{aligned}$$

where the factor 2 in the second equation results from the fact that $\widetilde{\varepsilon}$ is twice the symmetric gradient. The precise specifications are stated in the following example.

Example V.2. *Let* $\gamma = 1$*,* $\omega = (0,1)\times(-1/2, 1/2)$ *with clamped boundary conditions on* $\partial\omega$ *defined by traces of the functions*

$$u(x,y) = \frac{1}{4}\begin{bmatrix}0\\ -xy\end{bmatrix}, \quad w(x,y) = \frac{1}{2}x^2\sin y.$$

We have

$$g(x,y) = -\frac{1}{2}\begin{bmatrix} -1 + 8x\sin^2 y + 2x^3(\cos^2 y - \sin^2 y) \\ (6x^2 - 2x^4)\cos y \sin y \end{bmatrix}$$

and

$$\begin{aligned} f(x,y) =& \frac{\gamma^2}{2}[-4+x^2]\sin y - \frac{1}{4}\big(-4xy\cos y + 2[-x+x^3]\sin y\big) \\ & - \frac{1}{4}\big(4[6x^2-x^4]\sin^3 y + [10x^4+8x^4-3x^6]\sin y\cos^2 y\big). \end{aligned}$$

For a sequence of uniformly refined triangulations $\mathcal{T}_\ell$ obtained from a triangulation of ω into two triangles by carrying out ℓ red refinements, we ran Algorithm V.1 to compute a nearly stationary configuration (u_ℓ, w_ℓ) of the energy functional E_h specified in Example V.2. The discrete gradient flow was initialized with small perturbations of the interpolants of the exact solutions. For $\ell = 3, 4, \ldots, 7$ we computed the approximation errors

$$\delta_u^\ell = \|\widetilde{\varepsilon}(\mathcal{I}_\ell u - u_\ell)\|, \quad \delta_w^\ell = \|D_h^2(\mathcal{I}_\ell^{3,\mathrm{red}} w - w_\ell)\|$$

and displayed these numbers for different mesh sizes $\widehat{h}_\ell = h_\ell/\sqrt{2}$ in Table 1. The numbers reveal a nearly linear experimental convergence rate which coincides with the expected quasioptimal rate of convergence. The approximations (u_5, w_5) are displayed in Figure 2.

$\widehat{h}_\ell$	2^{-3}	2^{-4}	2^{-5}	2^{-6}	2^{-7}
δ_w^ℓ	0.027 255	0.014 168	0.007 205	0.003 629	0.001 820
δ_u^ℓ	0.006 592	0.003 758	0.001 871	0.000 944	0.000 478

TABLE 1. Approximation errors in Example V.2 for different mesh sizes. A nearly linear experimental order of convergence is observed.

V.B. **Compression along a clamped side.** We consider a plate that is attached on one side to an elastic substrate which is compressed in the direction parallel to the side, cf. Figure 3. We model this scenario by compressive clamped boundary conditions specified in the following example.

Example V.3. *Let* $\omega = (0,1)\times(-1/2,1/2)$ *and* $\gamma_{\mathrm{D}} = \{0\}\times[-1/2,1/2]$ *and set* $f = g = 0$ *and*

$$u_{\mathrm{D}}(x) = \begin{bmatrix} 0 \\ -x_2/10 \end{bmatrix}, \quad w_{\mathrm{D}}(x) = 0$$

for $x = (x_1, x_2) \in \omega$.

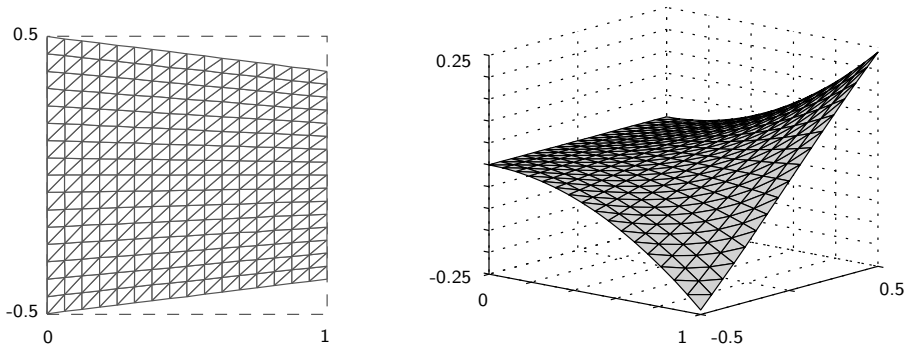

FIGURE 2. Numerical solution (u_5, w_5) in Example V.2. The in-plane deformation u_5 is shown in the left and the deflection w_5 in the right plot.

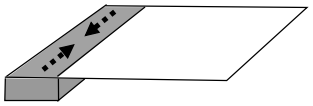

FIGURE 3. Illustration of the physical situation modeled in Example V.3.

We ran Algorithm V.1 in Example V.3 on uniform triangulations $\mathcal{T}_\ell$ with mesh sizes $\widehat{h}_\ell = h_\ell/\sqrt{2} = 2^{-\ell}$, $\ell = 5, 6, 7, 8$, resulting from ℓ uniform refinements of a reference triangulation $\mathcal{T}_0$. We initialized the iteration with the interpolants in the respective finite element spaces of the functions

$$\widetilde{u}_{\mathrm{D}}(x) = u_{\mathrm{D}}(x), \quad \widetilde{w}_{\mathrm{D}}(x) = \frac{1}{2}x_1^2(1-x_1)^2\sin(4\pi x_2)$$

which introduce out-of-plane oscillations in the initial deformation.
Figure 4 visualizes the numerical solution on the triangulation $\mathcal{T}_6$ for the thickness parameter $\gamma = 5.0 \cdot 10^{-3}$. We observe a folding structure along the compressed side of the plate. To understand the geometric properties of these structures we computed the solutions on the triangulations $\mathcal{T}_5, \mathcal{T}_6, \mathcal{T}_7, \mathcal{T}_8$ with the same fixed parameter $\gamma = 5.0 \cdot 10^{-3}$ and displayed top views of the deformations shaded by the corresponding bending energy densities $|D_h^2 w_h|$ in Figure 5. We observe that the frequency of the folding structure increases with decreasing mesh size but does not differ significantly for triangulations $\mathcal{T}_7$ and $\mathcal{T}_8$ reflecting the fact that the related length scale is determined by the paramter γ which is not sufficiently resolved on triangulations $\mathcal{T}_5$ and $\mathcal{T}_6$. The dependence of the length scale becomes apparent in Figure 6 where we displayed the numerical solutions in Example V.3 for the fixed triangulation $\mathcal{T}_7$ and the thickness parameters $\gamma = 1/10$, $1/40$, $1/160$, and $1/640$.
In the left plot of Figure 7 we compared the decay of the discrete elastic energy for our proposed adaptive step size strategy to the same iteration

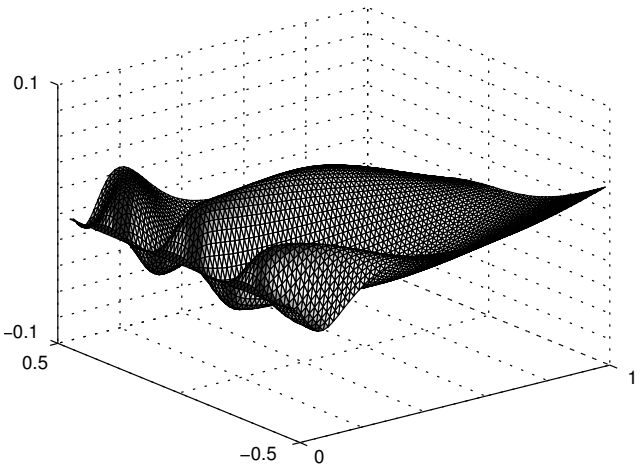

FIGURE 4. Numerical deformation on triangulation $\mathcal{T}_6$ shaded by bending energy density in Example V.3 for $\gamma = 5.0 \cdot 10^{-3}$.

with fixed step size $\tau = 1$. We observe that the adaptive strategy decreases the energy to a value $E_h(u_h^k, w_h^k) \approx 0.6 \cdot 10^{-3}$ within about 50 iterations of Algorithm V.1 while for uniform step sizes the iteration appears to get stuck at the energy level $E_h(u_h^k, w_h^k) \approx 4.0 \cdot 10^{-3}$. The adaptively generated step sizes are shown in the right plot of Figure 7. The initial step size $\tau_1 = 1$ is gradually increased until it reaches the maximal step size $\tau_{max} = 10^5$ after approximately 25 iterations when a nearly stationary configuration is found.

V.C. **Indentation of an elastic cone.** To describe the moderate elastic deformation of an initially nonflat elastic sheet, we include a term that models a prescribed stress in the flat reference configuration, i.e., we consider the modified Föppl–von Kármán functional

$$\widehat{E}(u,w) = \frac{\gamma^2}{2}\int_\omega |D^2 w|^2 \,\mathrm{d}x + \frac{1}{2}\int_\omega |\widetilde{\varepsilon}(u) + \nabla w \otimes \nabla w + \widehat{X}|^2 \,\mathrm{d}x.$$

To model the shape of a rescaled right circular cone $C \subset \mathbb{R}^3$ with flat base $B_{1/2}(0) \subset \mathbb{R}^2 \times \{0\}$ and apex $(0,0,1)$ we set $\omega = B_1(0)$ and

$$\widehat{X} = \frac{x^\perp \otimes x^\perp}{|x|^2}, \quad x^\perp = (-x_2, x_1).$$

The cone C is parametrized by the deformation $x \mapsto (x + \widehat{u}(x), \widehat{w}(x))$ defined by the in-plane-displacement and deflection

$$\widehat{u}(x) = -\frac{1}{2}x, \quad \widehat{w}(x) = 1 - |x|.$$

In particular for these functions the strain expression in $\widehat{E}$ vanishes, i.e., we have

$$\widetilde{\varepsilon}(\widehat{u}) + \nabla\widehat{w} \otimes \nabla\widehat{w} = -\widehat{X}.$$

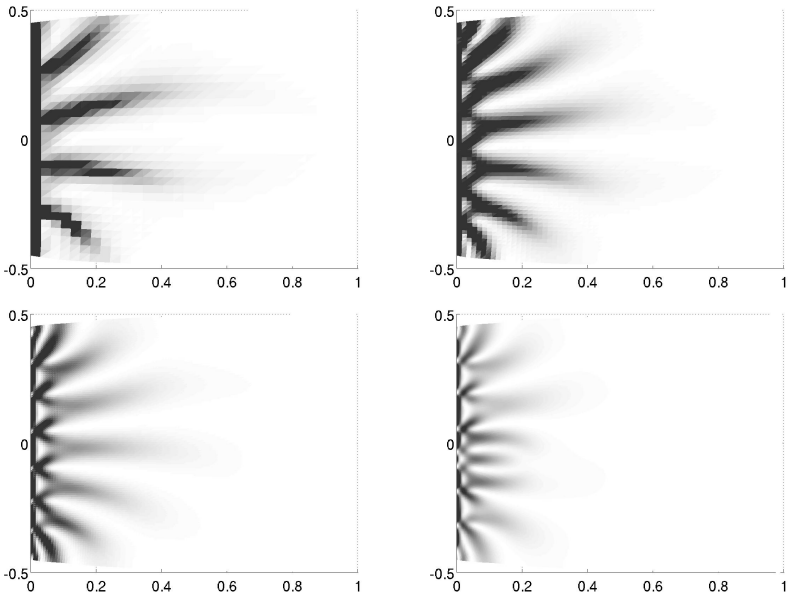

FIGURE 5. Numerical deformation and bending energy density in Example V.3 for fixed $\gamma = 5.0 \cdot 10^{-3}$ and triangulations with mesh sizes $\widehat{h}_\ell = 2^{-\ell}$, $\ell = 5, 6, 7, 8$.

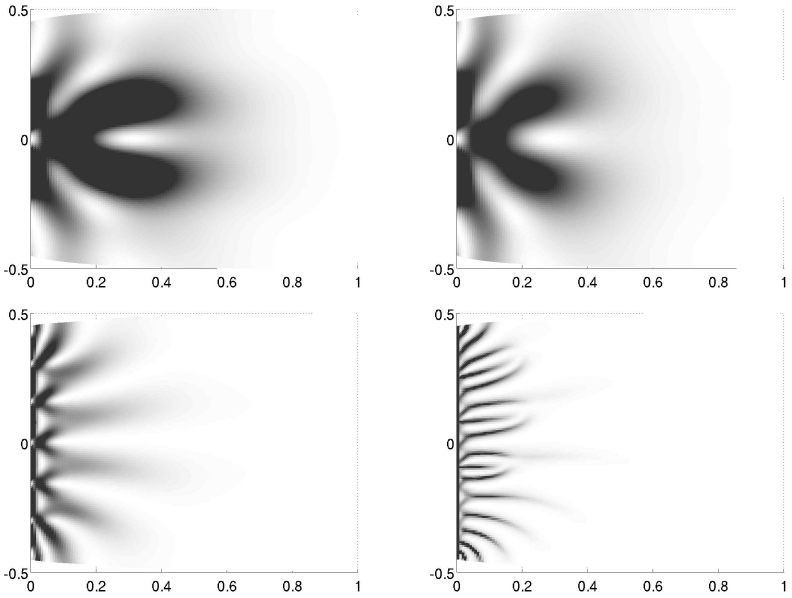

FIGURE 6. Numerical deformation and bending energy density in Example V.3 for $\gamma = 1/10$, $1/40$, $1/160$, and $1/640$ on the fixed triangulation $\mathcal{T}_7$.

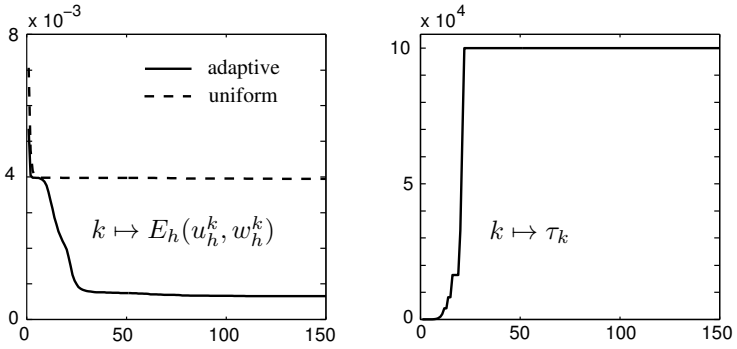

FIGURE 7. Energy decay for uniform and variable step sizes (left) and adaptively generated step sizes (right) in Example V.3 for $\gamma = 1/640$ and mesh size $h_7 \sim 2^{-7}$.

An energy minimizing configuration subject to appropriate boundary conditions would thus be a smoothed version of the cone depending on γ. Practically the cone can be imagined as being obtained from gluing together the noncircular sides of a half-disk of radius one. The following example models an indentation of the cone at its tip.

Example V.4. *For $\omega = B_1(0)$ and $0 \le \delta \le 2$ define $f = g = 0$ and*

$$u_{\mathrm{D}}(x) = -\frac{1}{2}x, \quad w_{\mathrm{D}}(x) = \min\big\{1 - |x|, |x| + (1-\delta)\big\}$$

and consider the clamped boundary condition on $\partial\omega$

$$u|_{\partial\omega} = u_{\mathrm{D}}|_{\partial\omega}, \quad w|_{\partial\omega} = w_{\mathrm{D}}|_{\partial\omega}, \quad \nabla w|_{\partial\omega} = \nabla w_{\mathrm{D}}|_{\partial\omega}$$

together with the indentation condition at the center $x_0 = 0$

$$w(0) = w_{\mathrm{D}}(0) = 1 - \delta.$$

For $\gamma = 1.0 \cdot 10^{-3}$ and an approximate triangulation $\mathcal{T}_5$ of the unit disk with $h_5 \sim 2^{-5}$ we displayed in Figure 8 the numerical deformations corresponding to the indentation strengths $\delta = 0.4, 0.6, 0.8, 1$. The numerical solutions appear to be rotationally symmetric but as shown analytically in [COT15] a break of symmetry occurs for certain indentation strengths. To visualize this instability we computed the numerical solution for $\delta = 0.8$ on the finer triangulation $\mathcal{T}_8$ with $h_8 \sim 2^{-8}$ and displayed in Figure 9 a magnification of the free boundary of the numerical solution along which a fold occurs. The observed instability is accompanied by nonuniquness of solutions and the selection mechanism acting here is defined by the chosen initial configuration and the geometric properties of the underlying triangulation.

Acknowledgments. The author is grateful to P. Dondl and H. Olbermann for stimulating discussions.

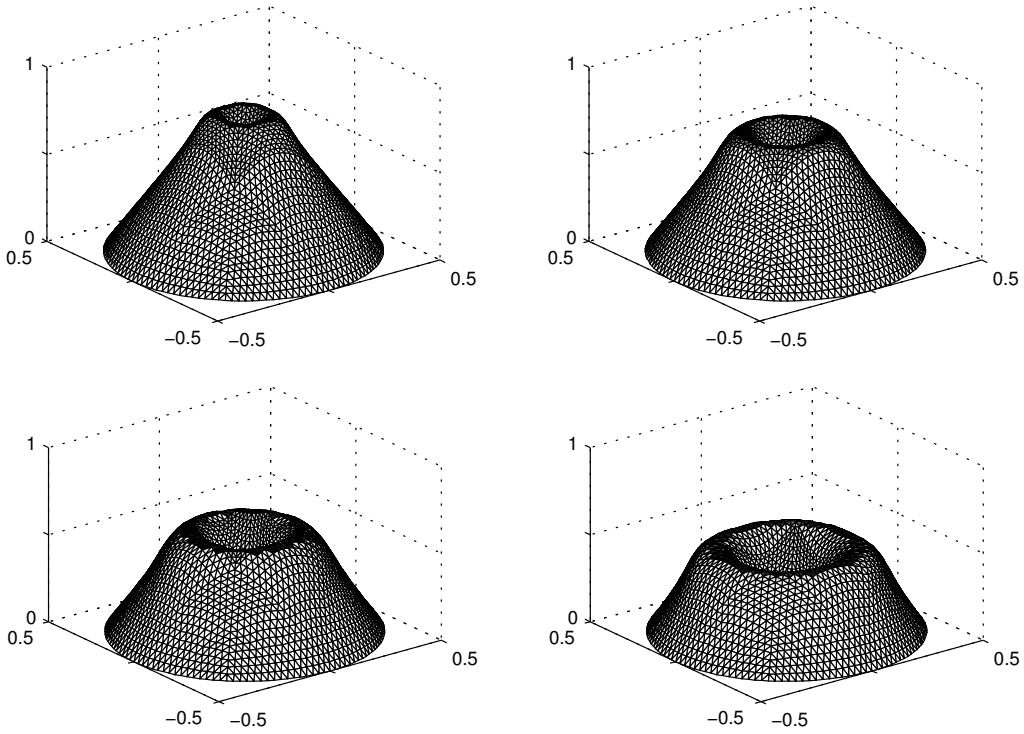

FIGURE 8. Numerical deformations for $\gamma = 1.0 \cdot 10^{-3}$ on a fixed triangulation $\mathcal{T}_5$ in Example V.4 with indentation strengths $\delta = 0.4, 0.6, 0.8, 1.0$.

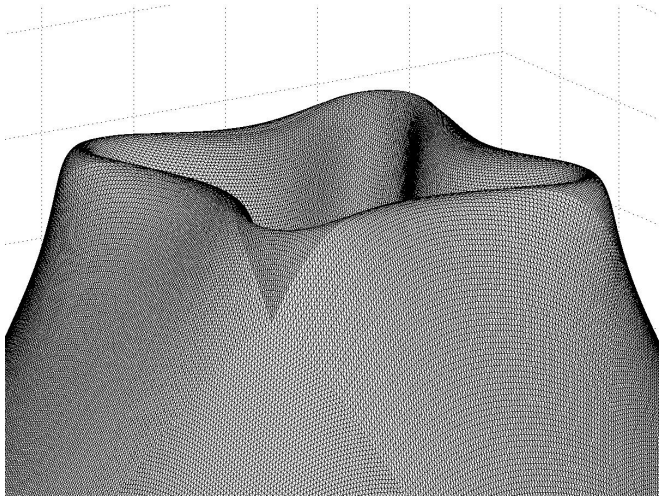

FIGURE 9. Magnification of the numerical deformation for $\gamma = 1.0 \cdot 10^{-3}$ and $\delta = 0.8$ on the triangulation $\mathcal{T}_8$ in Example V.4; a mesh dependent break of symmetry occurs.

References

[Bar13] Sören Bartels, *Approximation of large bending isometries with discrete Kirchhoff triangles*, SIAM J. Numer. Anal. **51** (2013), no. 1, 516–525.

[Bar15] ———, *Numerical methods for nonlinear partial differential equations*, Springer Series in Computational Mathematics, vol. 47, Springer, Cham, 2015.

[BBN15] Sören Bartels, Andrea Bonito, and Ricardo H. Nochetto, *Bilayer plates: Model reduction, γ-convergent finite element approximation, and discrete gradient flow*, Comm. Pure Appl. Math. (2015), n/a–n/a.

[BCM15] David Bourne, Sergio Conti, and Stefan Müller, *Folding patterns in partially delaminated thin films*, Innovative Numerical Approaches for Coupled Multi-Scale Problems (A. Pandolfi and K. Weinberg, eds.), Springer, 2015.

[Bel15] Peter Bella, *The transition between planar and wrinkled regions in a uniaxially stretched thin elastic film*, Arch. Ration. Mech. Anal. **216** (2015), no. 2, 623–672.

[BK14] Peter Bella and Robert V. Kohn, *Metric-induced wrinkling of a thin elastic sheet*, J. Nonlinear Sci. **24** (2014), no. 6, 1147–1176.

[Bra07] Dietrich Braess, *Finite elements*, third ed., Cambridge University Press, Cambridge, 2007.

[Bra14] Andrea Braides, *Local minimization, variational evolution and Γ-convergence*, Lecture Notes in Mathematics, vol. 2094, Springer, 2014.

[CGK07] Philippe G. Ciarlet, Liliana Gratie, and Srinivasan Kesavan, *On the generalized von Kármán equations and their approximation*, Math. Models Methods Appl. Sci. **17** (2007), no. 4, 617–633.

[Cia80] Philippe G. Ciarlet, *A justification of the von Kármán equations*, Arch. Rational Mech. Anal. **73** (1980), no. 4, 349–389.

[Cia97] ———, *Mathematical elasticity. Vol. II*, Studies in Mathematics and its Applications, vol. 27, North-Holland Publishing Co., Amsterdam, 1997.

[CM08] Sergio Conti and Francesco Maggi, *Confining thin elastic sheets and folding paper*, Arch. Ration. Mech. Anal. **187** (2008), no. 1, 1–48.

[COT15] Sergio Conti, Heiner Olbermann, and Ian Tobasco, *Symmetry breaking in indented elastic cones*, arXiv (2015), no. arXiv:1512.07029.

[DHR16] Patrick Dondl, Behrend Heeren, and Martin Rumpf, *Optimization of the branching pattern in coherent phase transitions*, arXiv (2016), no. arXiv:151206620.

[FJM02] Gero Friesecke, Richard D. James, and Stefan Müller, *The Föppl-von Kármán plate theory as a low energy Γ-limit of nonlinear elasticity*, C. R. Math. Acad. Sci. Paris **335** (2002), no. 2, 201–206.

[FJM06] ———, *A hierarchy of plate models derived from nonlinear elasticity by gamma-convergence*, Arch. Ration. Mech. Anal. **180** (2006), no. 2, 183–236.

[JC04] Stephen P. Jordan and Vincent H. Crespi, *Theory of carbon nanocones: Mechanical chiral inversion of a micron-scale three-dimensional object*, Phys. Rev. Lett. **93** (2004), 255504.

[KM94] Robert V. Kohn and Stefan Müller, *Surface energy and microstructure in coherent phase transitions*, Comm. Pure Appl. Math. **47** (1994), no. 4, 405–435.

[MO14] Stefan Müller and Heiner Olbermann, *Almost conical deformations of thin sheets with rotational symmetry*, SIAM J. Math. Anal. **46** (2014), no. 1, 25–44.

[NR14] Alice Nasto and Pedro M. Reis, *Localized structures in indented shells: A numerical investigation*, J. Appl. Mech **81** (2014), no. 12.

[Ven04] Shankar C. Venkataramani, *Lower bounds for the energy in a crumpled elastic sheet—a minimal ridge*, Nonlinearity **17** (2004), no. 1, 301–312.

Abteilung für Angewandte Mathematik, Albert-Ludwigs-Universität Freiburg, Hermann-Herder Str. 10, 79104 Freiburg i.Br., Germany